Computación y Sistemas Vol. 9 Núm. 4, pp. 355-369

Two Robust Techniques for Segmentation of Biomedical Images

Dos Técnicas Robustas para la Segmentación de Imágenes Biomédicas

Roberto Rodríguez, Patricio J. Castillo, Valia Guerra[1], Ana G. Suárez and Ebroul Izquierdo[2]

Digital Signal Processing Group
[1]Numerical Methods Group
Institute of Cybernetics, Mathematics & Physics (ICIMAF)
[2]Department of Electronic Engineering, Queen Mary, London University
rrm@icmf.inf.cu, vguerra@icmf.inf.cu, anagloria@icmf.inf.cu

Article received on October 15, 2004; accepted on August 18, 2006

Abstract

Image segmentation plays an important role in many systems of computer vision. According to criterions of many authors the segmentation finishes when it satisfies the goals of the observer. For that reason, an only method there is not able of solving all the problems that exists in the present time. In this work, we carry out a comparison between two segmentation techniques; namely, through the mean shift, where we give a new algorithm, and by using spectral methods. In the paper we discuss, through examples with biomedical real images, the advantages and disadvantages of them.
Keywords: Image segmentation, mean shift, spectral methods.

Resumen

La segmentación de imagen juega un importante rol en muchos sistemas de visión por computadora. Acorde al criterio de muchos autores la segmentación finaliza cuando son satisfechos los objetivos del observador. Por esa razón, no hay un único método capaz de resolver todos los problemas que existen en la época actual. En este trabajo, nosotros llevamos a cabo una comparación entre dos técnicas de segmentación; a saber, a través de la media desplazada, donde nosotros ofrecemos un nuevo algortimo, y usando los métodos espectrales. En el artículo nosotros discutimos, a través de ejemplos con imágenes biomédicas reales, las ventajas y desventajas de ellos.
Palabras claves: Segmentación de imagen, media desplazada, métodos espectrales

1 Introduction

Segmentation and contour extraction are important steps in many systems of high level. Segmented images are now used routinely in a multitude of different applications, such as, diagnosis, treatment planning, localization of pathology, study of anatomical structure, computer-integrated surgery, among others. However, image segmentation remains a difficult task due to both the variability of object shapes and the variation in image quality. Particularly, medical images are often corrupted by noise and sampling artifacts, which can cause considerable difficulties when applying rigid methods. Nevertheless, in spite of the most complex algorithms developed until present, segmentation continues being very dependent on the application and an only method there is not able of solving all the problems arising in the universe.

The pathological anatomy is a speciality, where the use of different techniques of digital image processing (DIP) allows improving the accuracy of the diagnosis of many diseases. One of the most important diseases in order to study today is the cancer, which constitutes one of the first causes of death in all those countries where the epidemics do not have an important weight.

Many segmentation methods have been proposed for medical-image data [1-6]. Unfortunately, segmentation using traditional low-level image processing techniques, such as thresholding, histogram, region growing and other classical operations requires a considerable amount of interactive guidance in order to attain satisfactory results. Automating these model-free approaches is difficult because of complexity, shadows, and variability within and across individual

objects. Furthermore, noise and other image artifacts can cause incorrect regions or boundary discontinuities in objects recovered from these methods.

A robust technique used in the present work was the mean shift, which is a nonparemetric procedure and it is an extremely versatile tool for feature analysis and can provide reliable solutions for many vision tasks [7, 8]. The mean shift was proposed in 1975 by Fukunaga and Hostetler [9] and largely forgotten until Cheng´s paper [10] rekindled interest in it. In spite of its excellent qualities, the mean shift procedure does not seem to be known in statistical literature.

The other technique used to carry out the comparison was the spectral methods, which is based on the calculation of the eigenvectors and eigenvalues of a matrix obtained from the affinities of the pixels in the image. In particular, it was used a spectral method called of *Normalized Cut* [11], which measures both total dissimilarity between the different groups as well as the total similarity within groups. The main idea is solving the eigenvalue problem for a small random subset of pixels (sample) and then extrapolating this solution to the full set of pixels. The theoretical aspects of the used methods are exposed in the developing of the work.

The paper is structured of the following way: in section 2 are given the details of the most significant theoretical aspects of each of the used methods. In section 3 the characteristics of the study images are described, and in section 4 the steps in the experimentation are explained. Here, we will carry out an analysis and discussion of both methods. Finally, in section 5 the most important conclusions are given.

2 Theoretical Aspects

2.1 The mean shift

Kernel density estimation (know as the Parzen window technique in pattern recognition literature [8]) is the most popular density estimation method. Given n data points x_i $i=1, \ldots, n$ in the d-dimensional space R^d , the *multivariate kernel density estimator* with kernel $K(x)$ and a symmetric positive definite dxd bandwidth matrix $\boldsymbol{H}$, computed in the point x is given by

$$\hat{f}(x) = \frac{1}{n}\sum_{i=1}^{n} K_H(x - x_i) \tag{1}$$

where,

$$K_H(x) = |H|^{\frac{-1}{2}} K\left(H^{\frac{-1}{2}} x\right) \tag{2}$$

Some considerations on matrix $\boldsymbol{H}$ and the mathematical background and other definitions can be found in [8]. Employing only one bandwidth parameter, the kernel density estimator in the expression (1) becomes the well-known expression

$$\hat{f}(x) = \frac{1}{nh^d}\sum_{i=1}^{n} K\left(\frac{x - x_i}{h}\right) \tag{3}$$

The quality of a kernel density estimator is measured by the mean of the square error between the density and its estimate, integrated over the domain of definition. In practice, however, only an asymptotic approximation on this measure can be computed [8].

A digital image can be represented as a two-dimensional array of p-dimensional vectors (pixels), where $\boldsymbol{p} = 1$ in the gray level case, three for color images, and $\boldsymbol{p} > 3$ in the multispectral case [8]. The space of the pixels is known as the *spatial* domain, while the gray level, color, or spectral information is represented in the *range* domain. For both domains, Euclidean metric is assumed. In this edition the case of gray level images will be only analyzed.

As was pointed in [8] when the location and range vectors are concatenated in the joint spatial-range domain of dimension $d = p+2$, their different nature has to be compensated by proper normalization with the h_s and h_r parameters. Thus, the multi-variable kernel is defined as the product of two radially symmetric kernels and the Euclidean metric allows a single bandwidth for each domain, that is,

$$K_{h_s, h_r}(x) = \frac{C}{h_s^2 h_r^p} k\left(\left\|\frac{x^s}{h_s}\right\|^2\right) k\left(\left\|\frac{x^r}{h_r}\right\|^2\right)$$

were x^s is the spatial part, x^r is the range part of a feature vector, $k(x)$ the common profile used in both domains, h_s and h_r the employed kernel bandwidths, and C the corresponding normalization constant.

The novelty lies in applying the mean shift procedure for the data points in the joint spatial-range domain. Each data point becomes associated to a point of convergence which represents the local mode of the density in the d-dimensional space. The process, having the parameters h_s and h_r, take into account simultaneously both the spatial and range information. For the segmentation task, the convergence points sufficiently close in the joint domain are fused to obtain the homogenous regions in the image.

2.1.1 Mean shift as normalized density gradient estimate

The iterative procedure of the mean shift is introduced as normalized density gradient estimate. By employing a differentiable kernel, an estimate of the density gradient can be defined as the gradient of the kernel density estimate; that is,

$$\hat{\nabla} f(x) \equiv \nabla \hat{f}(x) = \frac{1}{nh^d} \sum_{i=1}^{n} \nabla K\left(\frac{x - x_i}{h}\right) \tag{4}$$

Conditions on the kernel $K(x)$ and the window radio h to guarantee asymptotic unbiasedness, mean-square consistency, and uniform consistency of the estimate in the expression (4) are derived in [9].

For example, for *Epanechnikov* kernel ($K_E(x) = \begin{cases} 1/2\, c_d^{-1} (d+2)(1 - \|x\|^2) & \text{if } \|x\| < 1 \\ 0 & \text{otherwise} \end{cases}$)

where c_d is the volume of the d-dimensional sphere [8].

Then, for the *Epanechnikov* kernel the density gradient estimate in the expression (4) becomes,

$$\hat{\nabla} f_E(x) = \frac{1}{n(h^d c_d)} \cdot \frac{d+2}{h^2} \sum_{x_i \in S_h(x)} (x_i - x) = \frac{n_x}{n(h^d c_d)} \cdot \frac{d+2}{h^2} \left(\frac{1}{n_x} \sum_{x_i \in S_h(x)} (x_i - x) \right) \tag{5}$$

where the region $S_h(x)$ is a hypersphere of radius h having the volume $h^d c_d$ centered on $\mathbf{x}$, and containing n_x data points, that is, the uniform kernel [7, 8]. The last term in expression (5) is called the *sample mean shift*,

$$M_{h,U}(x) \equiv \frac{1}{n_x} \sum_{x_i \in S_h(x)} (x_i - x) = \frac{1}{n_x} \sum_{x_i \in S_h(x)} x_i - x \tag{6}$$

As it will be shown in section 2.1.1.1, using a kernel different form the *Epanechnikov* kernel for the derivation of the density gradient estimate results in a weighted mean computation in the expression (6).

The quantity $\frac{n_x}{n(h^d c_d)}$ is the kernel density estimate $\hat{f}_U(x)$ computed with the hypersphere $S_h(x)$, and thus we can write the expression (5) as,

$$\hat{\nabla} f_E(x) = \hat{f}_U(x) \cdot \frac{d+2}{h^2} M_{h,U}(x) \tag{7}$$

which yields,

$$M_{h,U}(x) = \frac{h^2}{d+2} \frac{\hat{\nabla} f_E(x)}{\hat{f}_U(x)} \tag{8}$$

The expression (5) shows that an estimate of the normalized gradient can be obtained by computing the sample mean shift in a uniform kernel centered on *x*. In addition, when this estimate is obtained with the *Epanechnikov* kernel, the mean shift vector has the direction of the gradient of the density estimate at *x*. As the mean shift vector always points towards the direction of the maximum increase in the density, it can define a path leading to a local density maximum; that is, to a mode of the density (see Fig. 1).

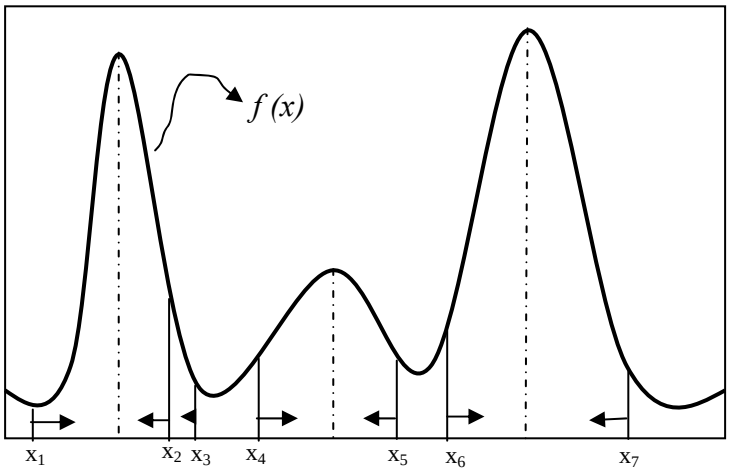

Fig. 1. Gradient mode clustering.

From expression (8) one can deduce that the normalized gradient introduces a desirable adaptive behavior, since the mean shift step is large for low density regions corresponding to valleys, and decreases as *x* approaches a mode. Mathematically, this is justified since $\frac{\hat{\nabla} f_E(x)}{\hat{f}_U(x)} > \hat{\nabla} f_E(x)$. Thus the corresponding step size for the same gradient will be greater than that near a mode. This will allow observations far from the mode or near a local minimum to move towards the mode faster than using $\hat{\nabla} f_E(x)$ alone.

The *mean shift procedure* obtained by successive

- computation of the mean shift vector $M_{h,U}(x)$ and
- translation of the window $S_h(x)$ by $M_{h,U}(x)$

is guaranteed to converge [7, 8, 10].

2.1.1.1 Generalization

Employing the profile notation, the density estimate in the expression (3) can be written as,

$$\hat{f}_K(x) = \frac{1}{nh^d}\sum_{i=1}^{n} k\left(\left\|\frac{x-x_i}{h}\right\|^2\right) \tag{9}$$

The first step in the analysis of a feature space with the underlying density *f(x)* is to find the modes of this density. The mode are located among the zeros of the gradient $\nabla f(x) = 0$ and the mean shift procedure in an elegant way to locate the zeros without estimating the density.

By denoting with $g = -k'$; that is, the profile defined by the derivative of profile *k* with the sign changed (we assume that the derivative of *k* exits $\forall x \in [0,\infty)$, excepting a finite set of points), then the density gradient estimate (see expression (4)) becomes,

$$\begin{aligned}\hat{\nabla} f_K(x) \equiv \nabla \hat{f}_K(x) &= \frac{2}{nh^{d+2}}\sum_{i=1}^{n}(x - x_i)k'\left(\left\|\frac{x-x_i}{h}\right\|^2\right) = \frac{2}{nh^{d+2}}\sum_{i=1}^{n}(x_i - x)g\left(\left\|\frac{x-x_i}{h}\right\|^2\right) \\ &= \frac{2}{nh^{d+2}}\left[\sum_{i=1}^{n} g\left(\left\|\frac{x-x_i}{h}\right\|^2\right)\right]\left[\frac{\sum_{i=1}^{n} x_i g\left(\left\|\frac{x-x_i}{h}\right\|^2\right)}{\sum_{i=1}^{n} g\left(\left\|\frac{x-x_i}{h}\right\|^2\right)} - x\right]\end{aligned} \tag{10}$$

where $\sum_{i=1}^{n} g\left(\left\|\frac{x-x_i}{h}\right\|^2\right)$ is assumed to be nonzero.

One can observe that the derivate of the *Epanechnikov* profile is the uniform profile, while the derivate of the normal profile remains as exponential.

The last bracket in expression (10) contains the mean shift vector computed with a kernel *G(x)* defined by $G(x) = cg\left(\|x\|^2\right)$, where *c* is a normalization constant; that is,

$$M_{h,G}(x) = \frac{\sum_{i=1}^{n} x_i g\left(\left\|\frac{x-x_i}{h}\right\|^2\right)}{\sum_{i=1}^{n} g\left(\left\|\frac{x-x_i}{h}\right\|^2\right)} - x = \frac{\sum_{i=1}^{n} x_i G\left(\frac{x-x_i}{h}\right)}{\sum_{i=1}^{n} G\left(\frac{x-x_i}{h}\right)} - x \tag{11}$$

Then, the density estimate at *x* becomes,

$$\hat{f}_G(x) = \frac{1}{nh^d}\sum_{i=1}^{n} G\left(\frac{x-x_i}{h}\right) = \frac{c}{nh^d}\sum_{i=1}^{n} g\left(\left\|\frac{x-x_i}{h}\right\|^2\right) \tag{12}$$

By using the expressions (11) y (12), the expression (10) becomes,

$$\hat{\nabla} f_K(x) = \hat{f}_G(x) \cdot \frac{2}{h^2 c} M_{h,G}(x) \tag{13}$$

from where the expression,

$$M_{h,G}(x) = \frac{h^2 c}{2} \frac{\hat{\nabla} f_K(x)}{\hat{f}_G(x)} \tag{14}$$

it is a generalization of the mean shift vector (see expression (8)). This allows using other kernels, for example, Gauss kernel, which gives wonderful results.

Basically, the algorithm that we use in this work has two steps, a filtering step and other, which is exactly the segmentation [11]. The filtered algorithm has the following steps [8]:

Let *Xi* and *Zi, i=1,..,n*, be the input and filtered images in the joint spatial-range domain. For each pixel $p \in Xi$, $p = (x, y, z) \in \Re^3$, where $(x, y) \in \Re^2$ and $z \in [0, 2^{\beta} - 1]$, β being the quantity of bits/pixel in the image.

1. Initialization
2. Compute the mean shift vector until convergence. We look for the mode, in which the mentioned pixel (*p*) converges. This can be carried out by using a uniform kernel o Gaussian. We used as stop criterion the absolute error.
3. Assign in *Zi* the *z* component of the calculated value (intensity of the level grey).

The steps of the proposed segmentation algorithm are the following:

1. Run the mean shift filtering procedure for the image and store all the information about the *d*-dimensional convergence point in z_i.

2. Define the regions that are in the spatial domain (hs) and that its intensities are smaller or equal than hr/2 (range domain).
3. For each of the defined regions in the step 2, one looks for all the pixels belonging to her and assigns in Z the mean of its intensity values.
4. Build the region graph through an adjacent list of the following way: for each region, one looks for all adjacent regions that are on the right hand side and below her.
5. While there exists nodes in the graph, which have been not visited, to run a variant of the "Depth-First Search" (DFS), which concatenates adjacent regions [11], where we gave as parameter a node, which has been not visited.
6. Go to the step 3 while is not obtained the stability (i. e, no more pixel value modifications).
7. Optional: Eliminate spatial regions containing less than *M* pixels, since those regions are considered irrelevant.
8. Optional (Binary): To all the pixels belonging to background, one assigns the white color and the black color to objects.

2.2 Spectral Methods

As have been pointed, spectral methods are based on the calculation of the eigenvectors and eigenvalues of a matrix derived from the affinities of the pixels in the image. Normalized Cut is a spectral method that measures both, total dissimilarity between the different groups as well as the total similarity within groups. The main difficulty of this method is the high dimension of the eigenproblem to be solved to natural images, which does not permit the use of standard techniques. A possible approach in this context is considering the image as a graph only locally connected imposing null values for the affinity between non-closed pixels, it guarantees an sparse structure for the affinity matrix and a considerable reduction of the time and memory computational cost of the problem.

However, it is not clear how the neglected affinities affect the image segmentation and techniques that involve dense affinity matrix promise better results. A spectral technique where all affinities are retained was proposed in [13]. The method is an extension of the *Nystrom* approximation for the integral eigenvalue problem. The main idea is solving the eigenvalue problem for a small random subset of pixels (sample) and then extrapolating this solution to the full set of pixels.

2.2.1 Normalized cut and Nystrom method

Let G be a set of pixels and let W be a weighted affinity matrix, then the method of Normalized Cut divides to G in two subsets G_1 and G_2 such that the normalized cut between them is minimum. The normalized cut is defined as,

$$Ncut(G_1, G_2) = \frac{2cut(G_1, G_2)}{vol(G_1) \,\|\, vol(G_2)} \tag{15}$$

where $cut(G_1,G_2)$ is the sum of the weights between G_1 and G_2, $vol\ (G_1)$ and $vol\ (G_2)$ is the sum of the degrees within the sets G_1 and G_2, respectively, and the symbol " $\|$ " denotes the harmonic mean.

The solution of this minimization problem can be approached by solving the standard eigenvalue problem following:

$$(D^{-1/2} W D^{-1/2}) V = \lambda V \tag{16}$$

where D is a diagonal matrix, $D_{ii} = \Sigma_j W_{ij}$ and $D^{-1/2}$ denotes the positive symmetric square root of the inverse of D. Basically, the *ith* component of the second largest eigenvector determines the embedding of the *ith* pixel. This process partitions the image in two disjointed sets.

Since the dimension N of W is the square of the G dimension, the solution of (16) involves a serious numerical difficulty when the problem is solved by a conventional equipment. The *Nystrom* extension is an efficient technique that uses the information of a subset of pixels in order to obtain an approximate solution of the eigenvalue problem. The extension of *Nystrom* is an efficient technique which uses the information of a subset of pixels in order to obtain an approximate solution of the eigenproblem.

For the sake of simplicity, the sample is defined as the first *n* pixels of the image matrix. The strategy consists of dividing the *W* matrix of the following way:

$$W = \begin{bmatrix} A & B \\ B^T & C \end{bmatrix} \tag{17}$$

and approximating the matrix W by a low-rank matrix,

$$\hat{W} = \begin{bmatrix} A & B \\ B^T & B^T A^{-1} B \end{bmatrix} \tag{18}$$

where the dimensions of the matrices *A* and *B* are *nxn* and *(nx(N-n)),* respectively, $n<<N$.

If *A* is a defined positive matrix, the second largest eigenvector of $\hat{W}$ can be estimated by calculating the second column of the V matrix, which is defined of the following way,

$$V = \begin{bmatrix} A \\ B^T \end{bmatrix} A^{-1/2} U_S \Lambda_S^{-1/2} \tag{19}$$

where U_S and Λ_S contain the spectral decomposition of the matrix,

$$S = A + A^{-1/2} B B^T A^{-1/2} \tag{20}$$

Note that the eigenproblem dimension is *n*, it implicates that if *n* is taken sufficiently small, the problem now can be solved to a suitable computation time.

It is clear to see that an interesting aspect of the algorithm is to know when the second largest eigenvector of $\hat{W}$ is a good approximation of the corresponding eigenvector of *W*. Although both vectors are theoretically different, the structure of the affinity matrix for natural images permits that generally $B^T A^{-1} B$ is a good approximation for the matrix *C*, and therefore the obtained segmentation by the method gives suitable results. The numerical experimentation carried out in [13] using the *Corel* data base, shows that roughly 100 randomly chosen samples are sufficient to capture the salient groups in typical natural images.

In this case, the elements of the used affinity matrix have the form,

$$W_{ij} = e^{-\frac{\|I_i - I_j\|^2}{\sigma_I}} * e^{-\frac{\|X_i - X_j\|^2}{\sigma_X}} \tag{21}$$

where X*i* is the spatial localization and *Ii* is the gray level of the *ith* node.

3 Features of the studied images

As biomedical images, we use biopsies, which represent histological cuts in malignant tumors. These were included in paraffin by using the inmunohistoquimic technique with the complex method of avidina biotina. Finally, monoclonal CD34 was contrasted with green methyl to accentuate new formation of blood vessels. These biopsies were obtained from human bodies of soft parts. This analysis was carried out for more of 80 patients. In Fig. 2 can be seen typical images, which were captured via MADIP system with a resolution of 512x512x8 bit/pixels [14].

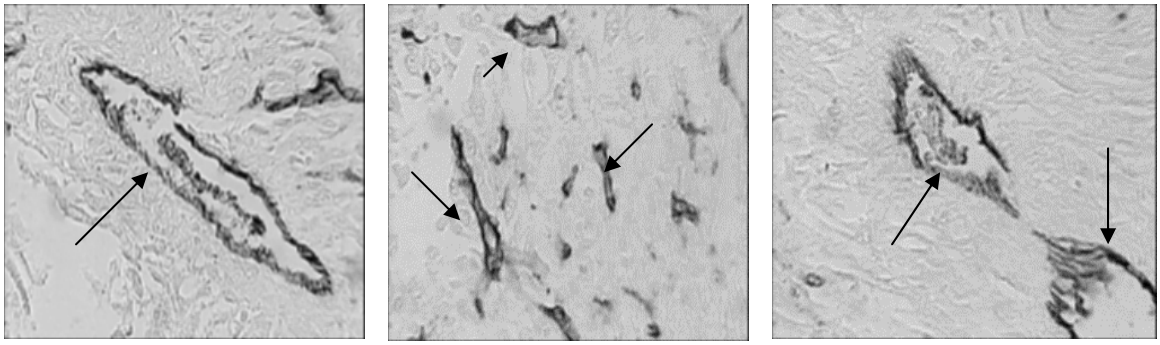

Fig. 2. These images represent the blood vessels in malignant tumors. Some blood vessels are marked with arrows.

In Fig. 3 can be observed a horizontal profile through the centre of a vessel; i. e., a plot of the pixel intensities along a single row.

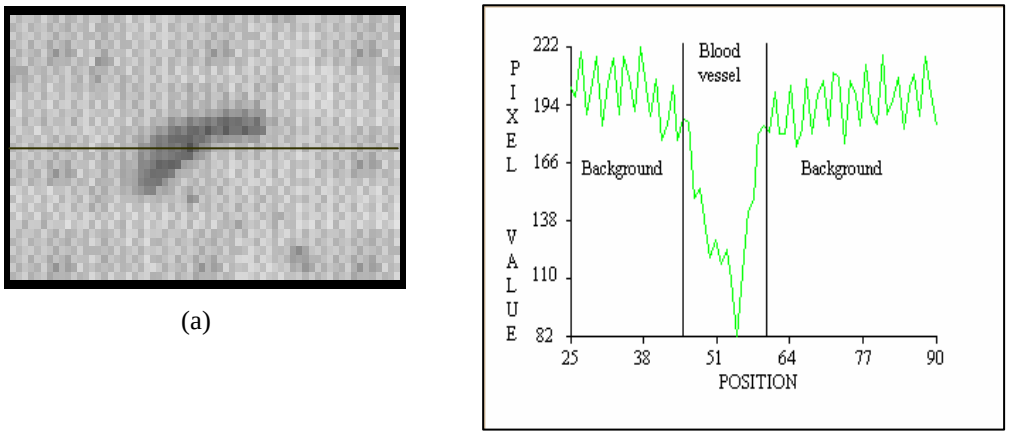

(a)

(b)

Fig. 3. An intensity profile through the centre of a vessel. Profile is indicated by a line in 3 (a).

There are several notable characteristics of these images, which are common to typical images that we encounter in the tissues of biopsies:

1. The intensity is slightly darker within the blood vessel than in the local surrounding background. It is emphasized that this observation holds only within the local surroundings.
2. High local variation of intensity is observed both within the blood vessel and the background. However, the local variation of intensity is higher within the blood vessel than in background regions (see Fig. 2(a)).

3. The variability of blood vessels both, in size and shape can be observed (see Fig. 2).

Due to acquisition protocol, the images are corrupted with a lot of noise.

4 Experimental Results. Analysis and Discussion

Now, we shall expose the obtained results in the blood vessels segmentation through the mean shift and a spectral technique, which was based on *Nystrom* method. In both methods the calculations were carried out by using *MATLAB* (ver. 6.5). In the case of the spectral method, the computational methods were elaborated by the authors and we included the modifications suggested in [15]. The size of the used sample was $n = 30$. In Fig. 4 a first example of this comparison is represented.

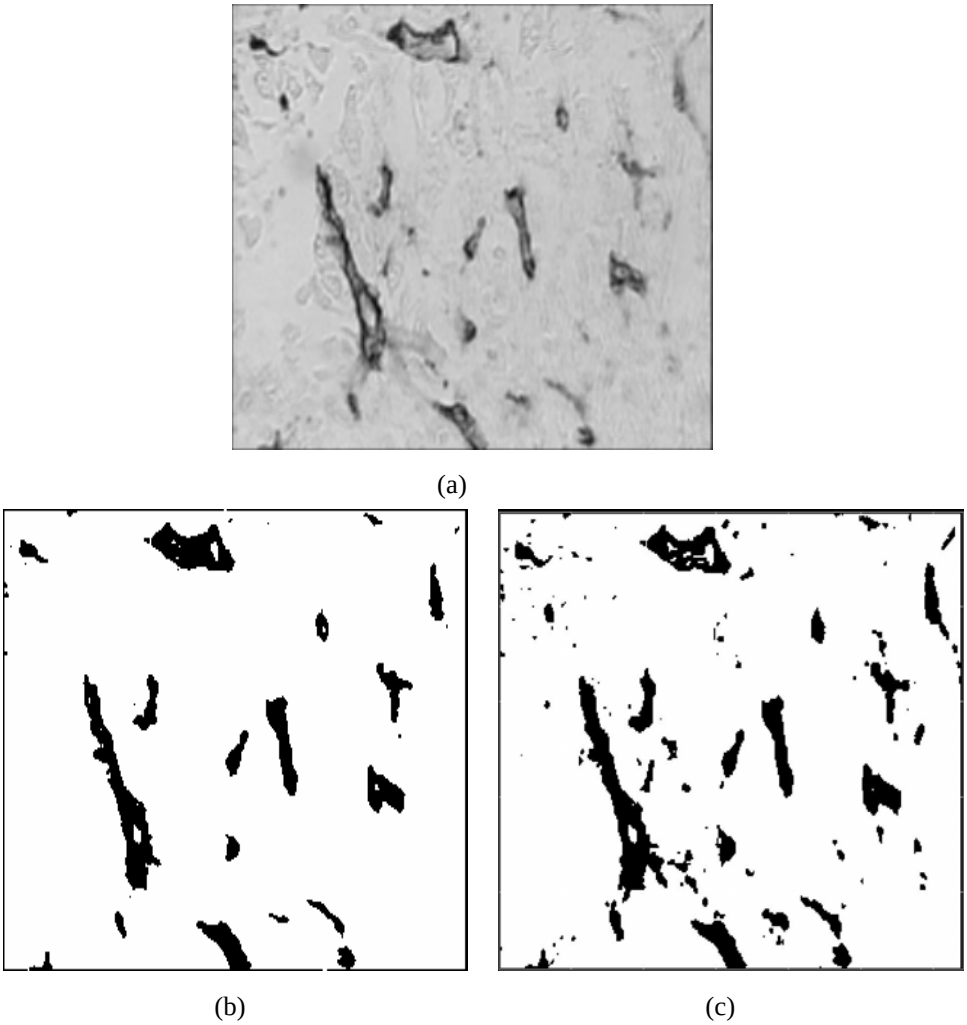

Fig. 4. (a) Original image, (b) Binary image by using the mean shift vector, (c) Obtained segmentation by the spectral method.

It is possible to observe (see Fig. 4) as the two methods were robust for the segmentation of histological images (in this case, blood vessels; but it was tested with other biomedical images). According to opinion of the physicians both

techniques were able of discriminating all blood vessels (BV), what it has much importance from point of view of the diagnostic. However, it can be seen that the obtained results with the mean shift were less noisy (see Fig. 4(b)). This is due by the effect of the used algorithm in the mean shift.

In Figs. 5, 6 and 7 appear other obtained results in the BV segmentation through the mean shift and with the spectral method.

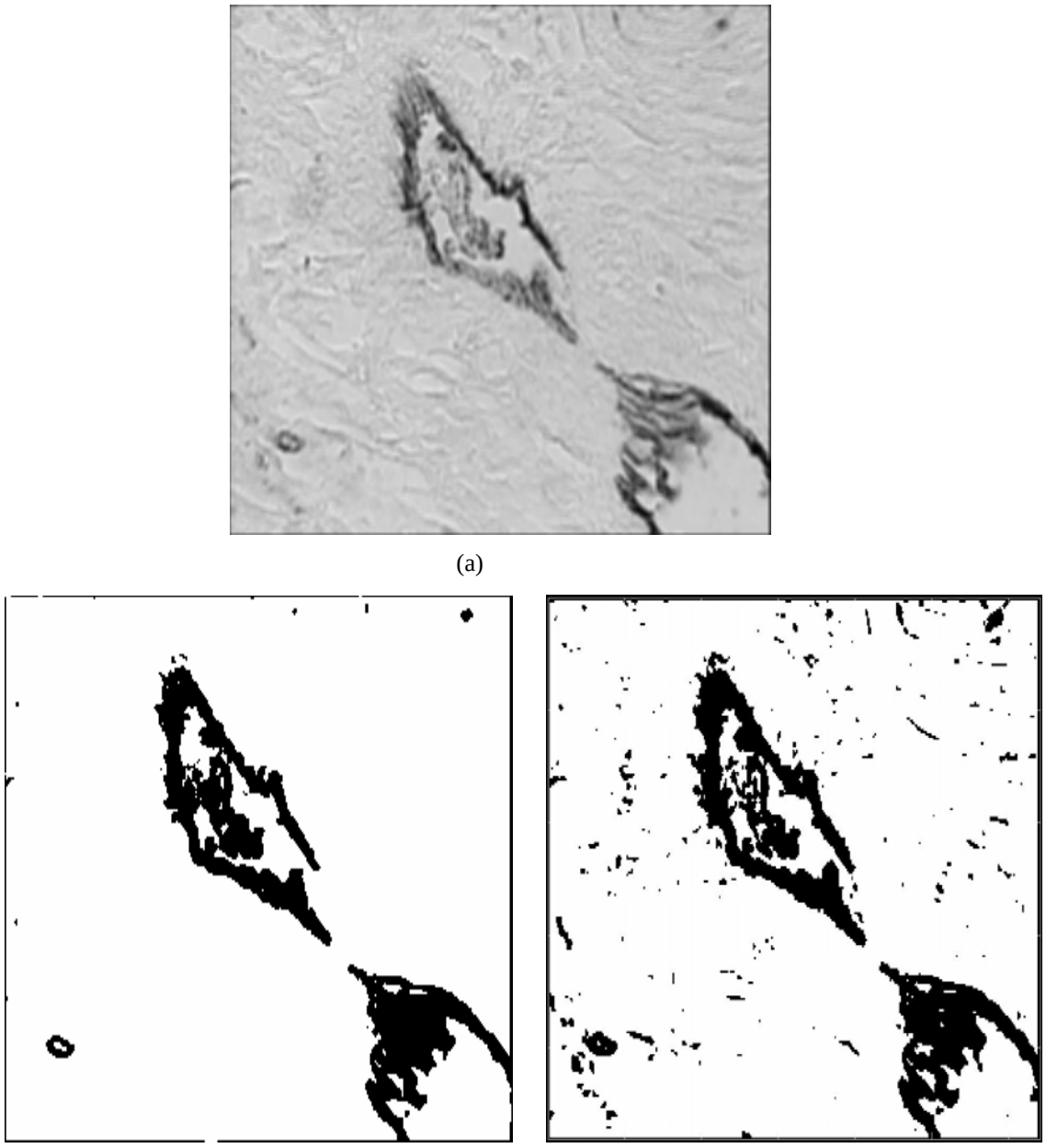

(a) (b) (c)

Fig. 5. (a) Original image, (b) Segmentation via the mean shift, (c) Obtained segmentation via the spectral method.

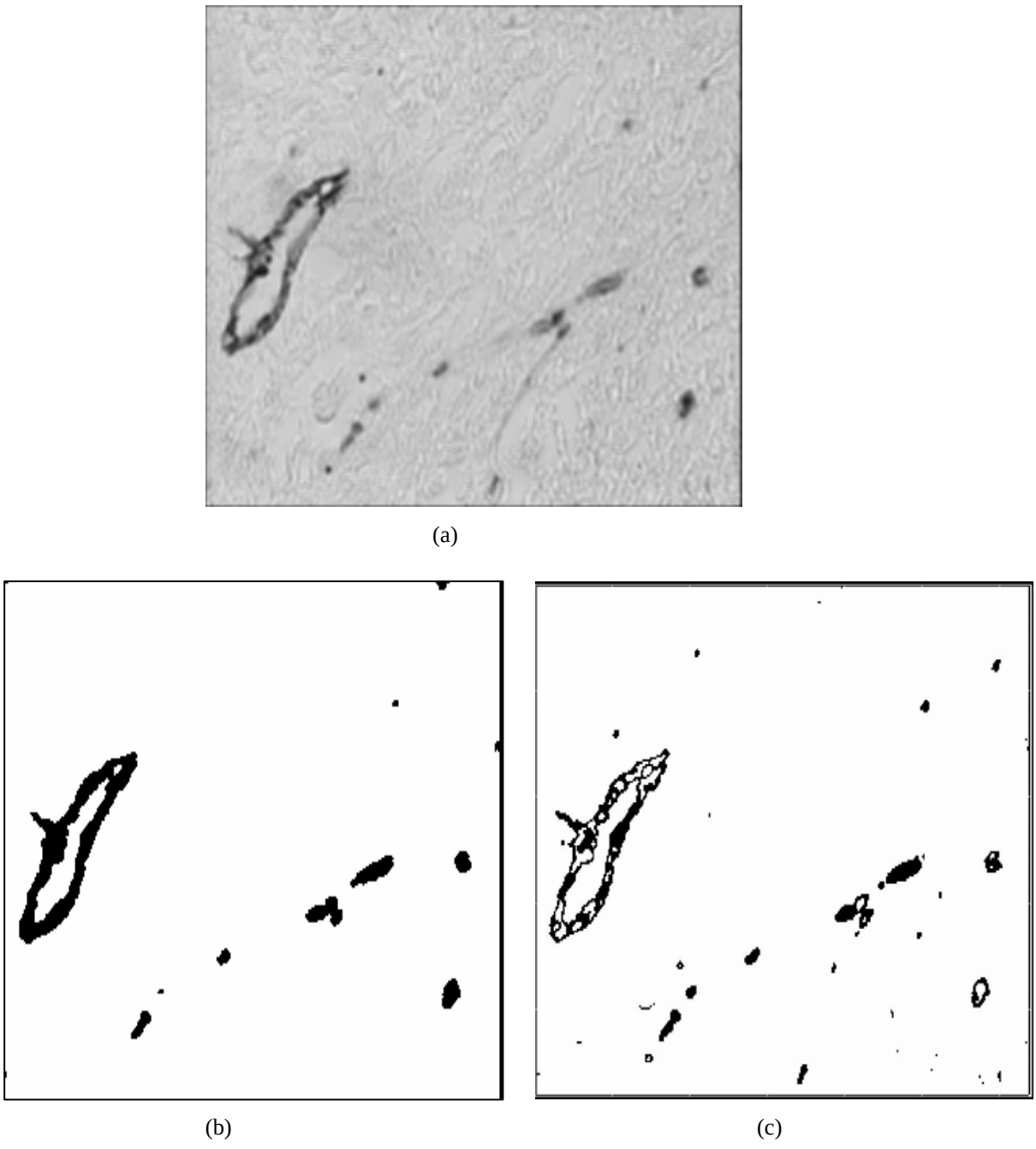

(a)

(b)

(c)

Fig. 6. (a) Original image, (b) Segmentation through the mean shift, (c) Obtained segmentation with the spectral method.

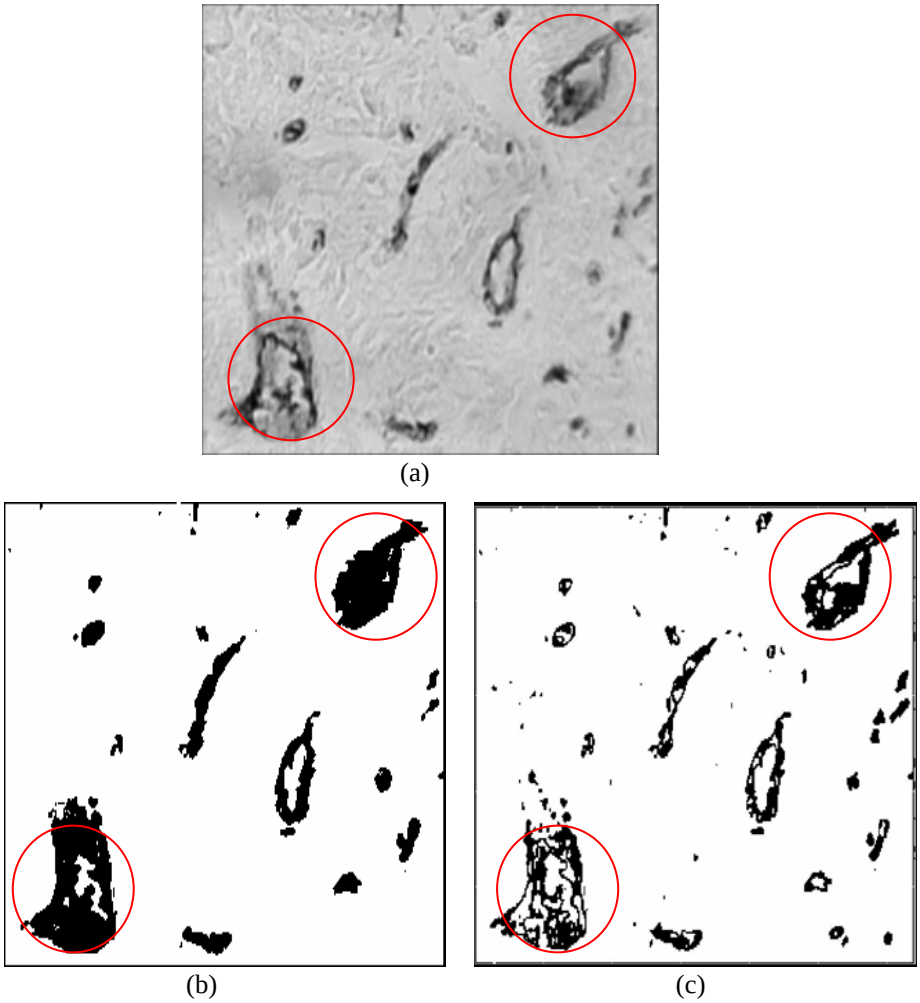

Fig. 7. (a) Original image, (b) Segmentation via the mean shift, (c) Segmentation via the spectral method. The circles mark the difference between the two methods.

In the presented examples, one can note as the two methods were able of isolating of effective way all the blood vessels. However, it can be observed that the segmented images with the mean shift algorithm were less noisy than the obtained images via the spectral method. In addition, the edges are noticed more robust and more defined in the images segmented with the mean shift (see circles in Fig. 7). In order to obtain more clear images with the spectral method is necessary to carry out an additional step with the goal of eliminating the spike noise which arises in the segmentation process. This procedure could be carried out through a morphological technique, which can be an opening or a majority filter. It is necessary to point out that this behavior was of this way for all the images which were processed.

From the point of view of algorithm, the mean shift is less complex than the spectral method and the segmentation process was carried out faster. In fact, in a Pentium IV to 2.6 GHz, the segmentation by the spectral method took 20 minutes, while that through the mean shift delayed running only 2 minutes.

5 Conclusions

In this work, we carried out a comparison between two robust technique of segmentation; namely, the mean shift and the spectral methods. We demonstrated by extensive experimentation, by using real image data, as the obtained images through the mean shift were less noisy than the spectral method. In addition, the obtained edges were more defined through the mean shift. It was tested that the algorithm of the mean shift was 10 times more rapid than the spectral method. These techniques can be extended to another biomedical images and its application is valid in other tasks where it are necessary to use robust methods of segmentation.

References

1. W. Kenong, D. Gauthier and M. D. Levine: "Live Cell Image Segmentation", IEEE Transactions on Biomedical Engineering, vol.42, no. 1, Jun. 1995.
2. J. Sijbers, P. Scheunders, M. Verhoye, A. Van der Linden, D. Van Dyck, E. Raman: "Watershed-based segmentation of 3D MR data for volume quatization", Magnetic Resonance Imaging, vol. 15, no. 6, pp 679-688, 1997.
3. C. Chin-Hsing, J. Lee, J. Wang and C. W. Mao: "Color image segmentation for bladder cancer diagnosis", Mathl. Comput. Modeling, vol. 27, no. 2, pp. 103-120, 1998.
4. Rodríguez, R., Alarcón, T., Wong, R. and Sanchez, L.: "Color segmentation applied to study of the angiogenesis. Part I", Journal of Intelligent and Robotic System, Vol. 34, No.1, May 2002.
5. P. Schmid: "Segmentation of digitized dermatoscopic images by two-dimensional color clustering", IEEE Trans. Med. Imag., vol. 18, no. 2, Feb., 1999.
6. J.E. Koss, F. D. Newman, T. K. Johnson and D. L. Kirch: "Abdominal organ segmentation using texture transforms and a hopfield neural network", IEEE Trans. Med. Imag., vol. 18, no. 7, July, 1999.
7. Comaniciu, D. I.: "Nonparametric Robust Method for Computer Vision", Ph.D. thesis, New Brunswick, Rutgers, The State University of New Jersey, January, 2000.
8. Comaniciu, D. and Meer, P.: "Mean Shift: A Robust Approach toward Feature Space Analysis", IEEE Transaction on Pattern Analysis and Machine Intelligence, Vol. 24, No. 5, May 2002.
9. Fukunaga, K. and Hostetler, L. D.: "The Estimation of the Gradient of a Density Function", IEEE Trans., Information Theory, Vol. 21, pp. 32-40, 1975.
10. Cheng, Y.: "Mean Shift, Mode Seeking, and Clustering", IEEE Trans., Pattern Analysis and Machine Intelligence, Vol. 17, No. 8, pp. 790-799, Aug. 1995.
11. Castillo, Patricio J.: "Robust Technique for Blood Vessels Segmentation in Malignant Tumors.", (In Spanish), Diploma Thesis, Mathematic Faculty, Havana University, 2004.
12. J. Shi and J. Malik, "Normalized Cuts and Image Segmentation", IEEE Trans. Pattern Analysis and Machine Intelligence, vol. 22, No. 8, pp. 888-905, 2000.
13. C. Fowlkes, S. Belongie, F. Chung, and J. Malik, "Spectral Grouping Using the Nystrom method," IEEE Trans. Pattern Analysis and Machine Intelligence, vol. 26, No. 2, pp. 214-225, 2004.
14. Rodríguez, R., Alarcón, T and Sánchez, L.**:** "*MADIP: Morphometrical Analysis by Digital Image Processing*", Proceedings of the IX Spanish Symposium on Pattern Recognition and Image Analysis, Vol. I, pp. 291-298, ISBN 84-8021-349-3, 2001, Spain.
15. E. Izquierdo and V. Guerra, "Numerical Stability of Nystrom Extension for Image Segmentation", Proceeding of 2004 IEEE International Workshop on Machine Learning for Signal Processing, Sept, 2004, Sao Luis, Brasil.

Roberto Rodríguez M. *received his diploma in Physic from the Physics Faculty, Havana University in 1978 and the PhD. Degree from Technical University of Havana, in 1995. Since 1998 he is the head of the Digital Signal Processing Group of the Institute of Cybernetics, Mathematics & Physics (ICIMAF). His research interests include Segmentation, Restoration, Mathematical Morphology, Visual pattern recognition, Analysis and Interpretation of images, Theoretical studies of Gaussian Scale-Space, New Lexis on Colour via Santana Method and Mean shift. He has published more than 40 articles in international journals and in many international conferences. He has received more of ten prizes as author and tutor.*

Valia Guerra *received the M.S and Ph.D degrees in Applied Mathematics from the University of Havana in 1995 and 1998, respectively. Currently, she is with the Numerical Methods Group of the Institute of Cybernetics, Mathematics and Physics,Havana, Cuba. Her research interests include Numerical Linear Algebra, Ill-posed problems and Regularization Methods.*

Ebroul Izquierdo *received the Ph.D. degree in mathematics from Humboldt University, Berlin, Germany, in 1993. He is the head of the Multimedia and Vision Research Group, Queen Mary. His research interests include stereo vision, efficient indexing and retrieval of video and information hidding in video signals. He is an Associated Editor of the IEEE Transactions on Circuits and Systems for Video Technology.*